Calibration and Cross-Tool Validation of 4H-SiC MOS n-Channel Inversion-Layer Mobility Models for Predictive TCAD Simulations

Huang Zhongtian
Power Electronics and Machines Centre, The University of Nottingham,
Nottingham, UK
ezxhz6@nottingham.ac.uk

Solon Christodoulou
Department of Electrical Engineering, and Computer Science and Engineering, Cyprus University of Technology
Limassol, Cyprus
ORCID: 0009-0001-3098-8537

Konstantinos Zaoskoufis
Department of Electrical Engineering, and Computer Science and Engineering, Cyprus University of Technology
Limassol, Cyprus
ORCID: 0000-0001-8047-0499

Paul Evans
Power Electronics and Machines Centre, The University of Nottingham,
Nottingham, UK
ORCID: 0000-0002-1693-417X

Munaf Rahimo
mqSemi AG
Zug, Switzerland
ORCID: 0000-0002-4632-5463

Iulian Nistor
mqSemi AG
Zug, Switzerland
iulian.nistor@mqsemi.com

Ke Li
Power Electronics and Machines Centre, The University of Nottingham,
Nottingham, UK
ORCID: 0000-0002-3190-1202

Neophytos Lophitis
Department of Electrical Engineering, and Computer Science and Engineering Cyprus University of Technology
Limassol, Cyprus
ORCID: 0000-0002-0901-0876

***Abstract*— Accurate channel-mobility reproduction is essential for predictive technology computer-aided design (TCAD) modelling of 4H-SiC MOSFETs, where inversion-layer transport is strongly degraded by interface-related scattering at the SiC/SiO_2 interface. This paper presents the calibration and validation of channel mobility in a planar 4H-SiC MOSFET structure using Synopsys Sentaurus and Silvaco. The effective mobility is evaluated by carrier-weighted extraction and calibrated against published reference mobility characteristics derived from lateral 4H-SiC MOSFET data over gate-bias, P-well-doping, and temperature variations. The results show that the calibrated implementations reproduce the expected channel-mobility trends and support predictive TCAD modelling of 4H-SiC MOSFETs.**

Keywords*— *4H-SiC MOSFETs, TCAD, inversion-layer mobility, remote Coulomb scattering, surface-phonon scattering, surface-roughness scattering

I. INTRODUCTION

Wide-bandgap (WBG) semiconductor devices enable higher switching frequency, improved efficiency, and increased power density in modern power-conversion systems. Among these devices, 4H-SiC MOSFETs are widely used in medium- and high-voltage applications such as on-board chargers, photovoltaic inverters, and traction converters [1], due to their high critical electric field, wide bandgap and strong thermal capability.

Predictive TCAD simulations are employed to support device design and performance evaluation in SiC power devices, but their accuracy depends strongly on the correct description of inversion-layer carrier transport, which is governed by the effective channel mobility μ_{eff}. In SiC MOSFETs, the mobility μ_{eff} is strongly degraded by interface-related scattering mechanisms at the SiC/SiO_2 interface [2], dominated by surface-roughness scattering (SR), surface-phonon scattering (SP), and remote Coulomb scattering (RCS) [3]. To account for these effects, a four-component mobility framework has been developed in which the mobility μ_{eff} is modelled as the harmonic sum of bulk mobility, surface-roughness scattering mobility μ_{SR}, surface-phonon scattering mobility μ_{SP} and remote Coulomb scattering mobility μ_{RCS}. In this work, the four-component mobility framework reported in [4] is implemented and calibrated both in Synopsys Sentaurus TCAD and in Silvaco TCAD, applied to a lateral planar 4H-SiC MOSFET structure, and evaluated across a P-well doping range of 3.6×10^{17}–1.0×10^{18} cm^{-3}. The objective is to demonstrate that the framework can be consistently implemented across different TCAD platforms while maintaining physically meaningful mobility behaviour in 4H-SiC MOSFET channel transport.

The interface mobility models employed in this work are adapted from the Si MOSFET literature, where inversion-layer transport has been extensively characterised [5], [6], [7]. The SR and SP scattering terms use functional forms originally introduced in the Lombardi concentration–voltage–temperature mobility (CVT) model [8], which was developed for Si/SiO2 interfaces. In Sentaurus, these terms are implemented through the standard CVT formulation recalibrated for SiC. In Silvaco, the alternative CVT (ALTCVT) model is used instead [9]: this is a 4H-SiC-specific alternative CVT model that uses acoustic-phonon and surface-roughness functional forms related to those in Lombardi, but with a modified SR exponent and a distinct bulk mobility expression. A key difference from the standard CVT model is that the Coulomb scattering term is included by default in ALTCVT, whereas it is excluded by default in the Lombardi model. Cross-tool validation is therefore particularly important, since the two environments implement these components through different internal model structures and parameter precedence rules, and small implementation differences can produce significant discrepancies in the extracted effective mobility if not carefully controlled.

The remainder of this paper is organised as follows. Section II describes the device structure, simulation setup, and mobility-extraction methodology. Section III presents the four-component mobility framework and the corresponding

Funded by the European Union under GA no. 101172794. Views and opinions expressed are however those of the authors only and do not necessarily reflect those of the European Union or CINEA. Neither the European Union nor the granting authority can be held responsible for them. This work was also supported by the Engineering and Physical Sciences Research Council (EPSRC), part of UK Research and Innovation (UKRI), under grant EP/X024377/1.

mobility-model implementations in Synopsys Sentaurus and Silvaco. Section IV presents the calibration strategy and validation results, while Section V discusses the extracted mobility components and the main findings. Section VI concludes the paper.

II. Device Structure, Mobility-Extraction Methodology, and Simulation Setup

A planar long-channel lateral 4H-SiC MOSFET, was used as the reference structure for channel-mobility extraction and calibration in both Synopsys Sentaurus TCAD [10] and Silvaco TCAD [11]. The device cross-section is shown in Fig. 1, where the N+ source and drain regions are placed on either side of the P-well channel, with no vertical drift region between the channel and the drain contact. The same two-dimensional device geometry was implemented in both environments, together with as closely aligned a set of physical models as possible, to enable a consistent comparison of the extracted channel mobility. This structure reduces the influence of bulk transport, anisotropic mobility, and drift-region resistance, such that the extracted mobility is governed primarily by transport at the SiC/SiO_2 interface. To maintain this channel-dominated operating condition, the simulations were performed under low-drain-bias conditions. The mobility was evaluated over the P-well doping range considered in this work in order to capture the doping dependence required for calibration of the model. Since the lateral structure contains no vertical drift region (Fig. 1) and the extraction is performed at VDS = 0 V, contributions from drift resistance and contact resistance to the extracted carrier-weighted mobility are absent.

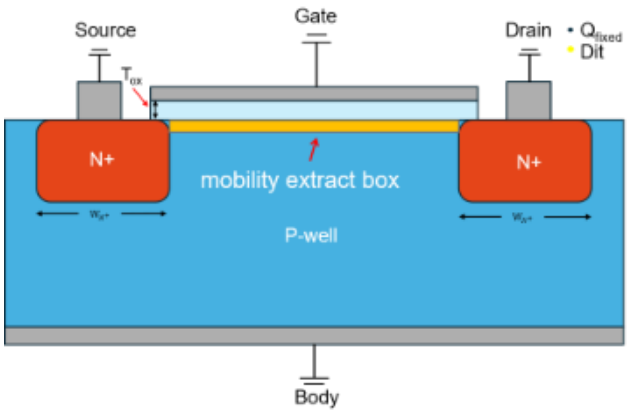


Fig. 1. Cross-sectional view of the simulated planar 4H-SiC MOSFET structure, showing the N+ source and drain regions, the P-well channel, the gate oxide, and the mobility extraction box positioned in the near-interface region beneath the gate.

The effective channel mobility was extracted from the TCAD solution using a carrier-weighted averaging method within a near-interface region underneath the gate oxide. The extraction region was chosen to include the inversion-layer carriers while excluding regions with negligible contribution to channel transport. In this work, the extraction box extends through the first 20 nm below the SiC/SiO_2 interface, which corresponds approximately to the spatial extent of the inversion layer under the applied bias conditions. The extraction was performed with $V_{DS} = 0$ V while V_{GS} was swept from 0 to 20 V.

Within the extraction region, the local electron concentration n and local electron mobility μ_n were obtained from the TCAD simulations and used to compute the effective channel mobility μ_{eff}according to:

$$\mu_{eff} = \frac{\int \mu_n(y) n(y) dy}{\int n(y) dy} \quad (1)$$

where $n(y)$ and $\mu_n(y)$ represent the electron concentration and the local electron mobility, respectively. This carrier-weighted definition provides a physically meaningful measure of inversion-layer transport because it naturally emphasises the parts of the channel where the conducting carriers are actually located. Accordingly, it provides a consistent basis for comparing the effective channel mobility extracted from Sentaurus and Silvaco. This definition originates from Si MOSFET inversion-layer studies [5], [6], and the same depth-integrated form applied within a near-interface TCAD extraction box is the procedure used in the reference work against which the present calibration is performed [4], [12].

In Synopsys Sentaurus, the carrier-weighted mobility can be evaluated directly within the TCAD workflow. In Silvaco, the same quantity was computed externally by extracting the spatial distributions of electron concentration and mobility, and processing them with a Python script that applies the same carrier-weighted expression. This preserves the same mobility-extraction definition in both environments. All simulations were performed under steady-state conditions in both TCAD environments. To ensure a consistent basis for channel-mobility extraction, the non-mobility physics settings were kept aligned across the two tools. These settings included conservative fixed interface charge, incomplete ionisation of dopants, high-field velocity saturation, and recombination through Shockley-Read-Hall and Auger recombination.

The two tools adopt different meshing strategies, which affects the resolution of the near-interface region and therefore the accuracy of the carrier-weighted extraction. In the Silvaco simulation, a non-uniform mesh is applied with increased line density near the SiC/SiO2 interface, where the inversion layer is spatially confined, transitioning to a coarser mesh deeper in the bulk. In the Sentaurus simulation, a non-uniform mesh is similarly applied over the full device domain, which spans a larger lateral and vertical extent. In both cases, the mesh density near the interface was verified to be sufficient to resolve the inversion-layer carrier distribution by confirming that further refinement produced no significant change in the extracted carrier-weighted mobility. This ensures that the reported effective mobility values are not sensitive to the specific meshing approach used by each tool.

III. Electron Channel-Mobility Model and Implementation

The effective channel mobility (μ_{eff}) is derived using Matthiessen's rule as,

$$\frac{1}{\mu_{eff}} = \frac{1}{\mu_{bulk}} + \frac{1}{\mu_{SR}} + \frac{1}{\mu_{SP}} + \frac{1}{\mu_{RCS}} \quad (2)$$

where μ_{bulk} denotes the bulk electron mobility, μ_{SR} the surface-roughness-limited mobility, μ_{SP} the surface-phonon-mobility, and μ_{RCS} the remote Coulomb scattering mobility. Each mobility component varies differently across the gate-bias range and influences a different region of the mobility characteristic, thereby providing the basis for subsequent

calibration against the published gate-bias, doping, and temperature trends.

A. Low field (Bulk) Mobility

The bulk electron mobility, μ_{bulk}, defines the baseline low-field electron mobility as a function of doping concentration and temperature. In this work, the unified Phillips/Klaassen model [13], [14] was used rather than a simpler Caughey–Thomas (CT) approach, because it provides a more suitable description of the doping- and temperature-dependent mobility behaviour [12]. It is described by eqs. (3)–(7), where $\mu_{\max}$ and $\mu_{\min}$ define the low- and high-doping mobility limits, N_{ref} sets the characteristic doping for mobility degradation, and $\theta$and αgovern the temperature dependence and the coupled doping–temperature behaviour. In the standard Lombardi CVT formulation the bulk mobility term is sometimes used to account for both lattice scattering and ionised-impurity Coulomb scattering in the channel. In the present framework this is explicitly separated: the Klaassen model describes only bulk ionised-impurity and carrier-carrier scattering through the Nsc,eff screening term, while all Coulomb scattering from interface charges and traps at the SiC/SiO2 interface is handled exclusively by the dedicated RCS term described in Section III-C.

$$\frac{1}{\mu_{bulk}} = \frac{1}{\mu_L} + \frac{1}{\mu_{DAeh}} \tag{3}$$

$$\mu_L = \mu_{max}\left(\frac{T}{300K}\right)^{-\theta} \tag{4}$$

$$\mu_{DAeh} = \mu_N\left(\frac{N_{sc}}{N_{sc,eff}}\right)\left(\frac{N_{ref}}{N_{sc}}\right)^{\alpha} + \mu_c\left(\frac{n+p}{N_{sc,eff}}\right) \tag{5}$$

$$\mu_N = \frac{\mu_{max}^2}{\mu_{max}-\mu_{min}}\left(\frac{T}{300K}\right)^{3\alpha-1.5} \tag{6}$$

$$\mu_c = \frac{\mu_{max}\mu_{min}}{\mu_{max}-\mu_{min}}\left(\frac{300K}{T}\right)^{0.5} \tag{7}$$

B. Surface-Roughness and Surface-Phonon mobility

The surface-roughness and surface-phonon scattering mobilities, μ_{SR} and μ_{SP}, are described using Lombardi-type functional forms [8]. In Sentaurus these are implemented via the standard CVT formulation. In Silvaco, the ALTCVT model is used: the SP term follows the same acoustic-phonon form as the Lombardi model, while the SR term uses a similar but not identical expression with a fixed exponent on the first term rather than the variable exponent in the Lombardi formulation. The SR term, given by (9), captures the mobility reduction associated with increased carrier confinement near the SiC/SiO_2 interface at higher gate bias, while the SP term, given by (10), describes the phonon-related limitation that shapes the mobility behaviour in the moderate- and strong-inversion regimes. The SR parameters δ, η, A, and ν control the magnitude and bias dependence of the roughness-related degradation, where A and ν set the field exponents governing the high-field roll-off, whereas the SP parameters B, C, and λ govern the mobility level, curvature, and doping sensitivity of the phonon-related contribution. In (8), the symbol μLomb denotes the combined surface-limited mobility from the SR and SP terms, irrespective of whether the standard CVT or the ALTCVT implementation is used.

$$\frac{1}{\mu_{Lomb}} = \frac{1}{\mu_{SR}} + \frac{1}{\mu_{SP}} \tag{8}$$

$$\mu_{SR} = \left[\frac{\left(\frac{F_\perp}{F_{ref}}\right)^{A^*}}{\delta} + \frac{F_\perp^3}{\eta}\right]^{-1} \tag{9}$$

$$\mu_{SP} = \frac{B}{F_\perp} + \frac{C\left(\frac{N_{A,0}+N_{D,0}+N_2}{N_0}\right)^{\lambda}}{F_\perp^{1/3}\left(\frac{T}{300K}\right)^{k}}. \tag{10}$$

C. Remote Coulomb scattering mobility

The remote Coulomb scattering mobility, μ_{RCS}, captures the mobility reduction associated with interface-related charges and traps near the SiC/SiO_2 interface [15]. This term is especially important at low gate bias, where Coulomb scattering strongly limits the effective channel mobility before being progressively screened as the inversion charge increases. Sentaurus and Silvaco use different equation sets and parameter definitions for this contribution, given here by (11) – (15) and (16) – (24), respectively.

The Sentaurus RCS model given by (11)–(15), $N_{A,D}$ is the effective channel doping concentration used by the model, $T$is the lattice temperature, $F_\perp$ is the transverse electric field at the interface, and N_{depl} is a depletion-related concentration term.

$$\mu_{RCS} = \frac{A_1\,A_2}{f(F_\perp)} \tag{11}$$

$$A_1 = \mu_{rcs0}\left(\frac{N_{A,D}}{3\times10^{16}\,cm^{-3}}\right)^{\gamma_1}\left(\frac{T}{300K}\right)^{\gamma_2} \tag{12}$$

$$A_2 = \left(g_{screening}\right)^{\gamma_3+\gamma_4\ln\left(\frac{N_{A,D}}{3\times10^{16}\,cm^{-3}}\right)} \tag{13}$$

$$g_{screening} = s + \frac{c}{c_0\left(\frac{N_{A,D}}{3\times10^{16}\,cm^{-3}}\right)^{\gamma_5}} \tag{14}$$

$$f(F_\perp) = 1 - \exp\left(-\xi\frac{F_\perp}{N_{depl}}\right). \tag{15}$$

The equations for the Silvaco remote Coulomb scattering model are (16)–(24), where n is the electron concentration, $|E_\perp|$ is the magnitude of the transverse electric field, T_L is the lattice temperature, and η is a scaled charge density term associated with one of the Coulomb-scattering charge sources.

$$\mu_{RCS} = \frac{N_{mob}\;Z_1\,Z_2}{Y_1\;Y_2} \tag{16}$$

$$Z_1 = \left(1+\frac{n}{N_{CT}\,\eta^{N_{P1}}}\right)^{(N_{NU})} \tag{17}$$

$$Z_2 = \left(\frac{T_L}{300K}\right)^{(N_{KT})} \tag{18}$$

$$Y_1 = 1 - exp\left[-\left(\frac{|E_\perp|}{E_{0N}}\right)^{(N_{GAM})}\right] \tag{19}$$

$$Y_2 = \eta^{(N_{P2})} \tag{20}$$

For electrons, three charge sources are considered, the channel acceptor density, the negative interface charge density, and the positive interface charge density. These are represented by the scaled quantities $\eta_A = \frac{N_A}{N_{TD}}$ (21) , $\eta_{n,n} = \frac{N_n}{N_{TT}}$ (22) and

$\eta_{n,p} = \frac{N_p}{N_{TT}}$ (23) respectively. In the Silvaco model, the interface-charge terms may include both fixed charge and trap-related charge at the SiC/SiO_2 interface. The three corresponding Coulomb-limited mobility terms are then combined using Matthiessen's rule to obtain the overall electron remote Coulomb scattering mobility, $\mu_{n,\mathrm{coul}}$.

$$\frac{1}{\mu_{n,coul}} = \frac{1}{\mu_n(\eta_A)} + \frac{1}{\mu_n(\eta_{n,n})} + \frac{1}{\mu_n(\eta_{n,p})} \qquad (24)$$

IV. Calibration and Validation

A. Calibration Strategy and Calibrated Parameter Sets

Calibration was performed sequentially with the primary validation target being to reproduce the effective channel mobility as a function of gate bias, P-well concentration, and temperature. First, the bulk mobility parameters were selected to reproduce the required doping- and temperature-dependent baseline behaviour reported in [2]. Next, the calibration targeted the reference mobility characteristics reported for lateral 4H-SiC MOSFET test structures in [4], focusing on the P-well concentration range of approximately 3.6×10^{17} to $1.0 \times 10^{18}\ \mathrm{cm}^{-3}$ and on the corresponding temperature dependence from 25 to 175°C. The surface-roughness and surface-phonon parameters were tuned to reproduce the shape and curvature of the effective mobility in the moderate- and strong-inversion regimes. Finally, the RCS parameters were calibrated to reproduce the low-V_G mobility limitation and its dependence on channel doping and inversion-charge screening. The calibrated parameter values are listed in Table I.

TABLE I: 4H-SiC MOSFET MOBILITY MODEL PARAMETERS

Bulk Mobility (3) - (7)			
Symbol	***Value***	***Units***	***Description***
μ_{max}	1010	cm^2/Vs	Maximum mobility at low doping
μ_{min}	40	cm^2/Vs	Minimum mobility at high doping
θ	2.93	-	Temperature coefficient
α	0.64	-	Doping/temperature coefficient
N_{ref}	1.6×10^{17}	cm^{-3}	Reference doping for mobility degradation

Surface Roughness (SR) Scattering (9)			
Symbol	***Value***	***Units***	***Description***
δ	1×10^{15}	cm^2/Vs	Low-field SR degradation
η	1×10^{22}	$V^2cm^{-1}s^{-1}$	High-field SR degradation
A	2	-	Low-field tuning factor
ν	1	-	Tuning parameter

Surface Phonon (SP) Scattering (10)			
B	1.2×10^{7}	cm/s	Low-field SP degradation
C	40	$cm^{5/3}V^{-2/3}s^{-1}$	High-field SP degradation
λ	0.125	-	Doping influence factor

Remote Coulomb Scattering (Sentaurus) (11) - (15)			
s	50	-	Low-field Coulomb factor
μrcs0	0.05	cm^2/Vs	Global scaling factor
γ_1	-1.5	-	Doping adaptation factor
γ_2	2.1	-	Temperature adaptation factor
γ_3	0.97	-	Post-inversion slope factor
γ_4	0.2	-	Doping-dependent slope factor
γ_5	1	-	Threshold-voltage dependence
ξ	1×10^{12}	$V^{-1}cm^{-1}$	Channel inversion criterion
c_0	1×10^{16}	cm^{-3}	Inversion carrier density

Remote Coulomb Scattering (Silvaco) (16) – (24)			
N_{mob}	2.2	$cm^2/V\cdot s$	Global Coulomb mobility scale
N_{KT}	1.8	-	Temperature dependence control
N_{TT}	7×10^{10}	cm^{-2}	Interface/oxide charge density factor
N_{TD}	1.7×10^{16}	cm^{-3}	Doping/reference concentration factor
N_{P1}	0.7	-	Shape control (weak–moderate inversion)
N_{P2}	0.8	-	Shape control (moderate–strong inversion)
N_{CT}	3.2×10^{17}	cm^{-3}	Screening/transition concentration
N_{NU}	1.21	-	Post-inversion slope control
E_{0N}	1×10^{4}	V/cm	Field scale parameter
N_{GAM}	1	-	Additional slope/shape factor

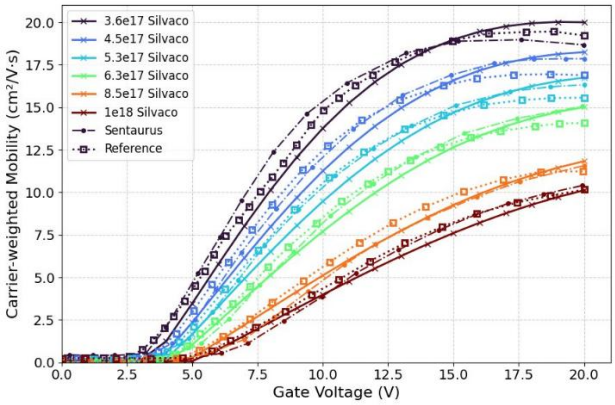


Fig. 2. Effective channel mobility, μ_{eff}, as a function of gate voltage, V_G, for different P-well doping concentrations, comparing the calibrated Synopsys Sentaurus and Silvaco results with the reference characteristics reported in [4].

B. Validation

Figure 2 compares the effective channel mobility predicted by Synopsys Sentaurus and Silvaco with the corresponding reference characteristics from [4] for different P-well doping concentrations. In all cases, both tools reproduce the main features of the $\mu_{\mathrm{eff}} - V_G$ behaviour, namely low mobility at small gate bias, a rapid increase following channel formation, and gradual saturation at higher V_G. The calibrated models also capture the reduction in mobility with increasing P-well doping, consistent with stronger Coulomb- and impurity-related scattering in the channel. Although small deviations remain in the turn-on and high-V_G regions, the overall agreement confirms that both TCAD implementations provide a consistent description of the doping-dependent inversion-channel mobility.

Figure 3 shows the corresponding temperature-dependent mobility behaviour for a representative high-doping case, together with the reference data. For all temperatures, the extracted effective mobility remains low at small V_G, increases rapidly after channel formation, and then gradually approaches saturation at higher gate bias. As temperature increases, the mobility curves shift upward and reach a higher saturation level, reproducing the same overall trend reported in the reference work. The calibrated simulations therefore capture the temperature dependence of inversion-layer transport in addition to its doping dependence. The largest deviations are observed near the turn-on region and, in some cases, in the high-V_G saturation regime, where the extracted mobility is particularly sensitive to the local inversion-charge distribution, interface-charge assumptions, and numerical resolution near the interface. Nevertheless, the overall agreement indicates that the calibrated model provides a consistent description of effective channel mobility across the temperature range considered.

V. Mobility-Component Analysis and Discussion

Both the Synopsys Sentaurus and the Silvaco implementations reproduce the expected physical trends and provide a consistent basis for predictive TCAD modelling of channel transport in 4H-SiC MOSFETs. The broader validation results show that this calibrated framework remains consistent across the full range of P-well doping and temperature considered in this work. Figure 2 confirms that both tools reproduce the expected reduction in effective mobility with increasing P-well concentration, as well as the corresponding variation in the shape of the $\mu_{\text{eff}} - V_G$ characteristics. Figure 3 further shows that the calibrated model captures the temperature dependence of the mobility curves, including the increase in mobility level and saturation value with increasing temperature reported in the reference data. Together, these results indicate that the calibration provides a consistent description of inversion-layer transport across gate bias, channel doping, and temperature.

Figure 4 shows the extracted mobility components and their Matthiessen's-rule combination as a function of gate voltage for the representative lowest-doped P-well case used in the calibration. This decomposition links the observed $\mu_{\text{eff}} - V_G$ behaviour to the underlying calibrated scattering terms and shows how the dominant channel-limiting mechanism evolves with gate bias. The behaviour can be interpreted by considering three gate-bias regimes:

- **Low V_G (weak inversion) -** At low V_G, the effective mobility is controlled primarily by remote Coulomb scattering, since the Coulomb-limited mobility is much smaller than the bulk-, surface-phonon-, and surface-roughness-limited components. This indicates that, in weak inversion, transport is dominated by scattering associated with interface-related charges before sufficient inversion charge is established to provide effective screening.

- **Moderate V_G (moderate inversion)** - As V_G increases beyond channel formation, the effective mobility rises rapidly because the Coulomb-limited mobility increases strongly with gate bias. This reflects progressive screening of the interface-related charges by the inversion layer. In this regime, the low- and moderate-V_G behaviour is therefore governed mainly by the remote Coulomb scattering contribution.

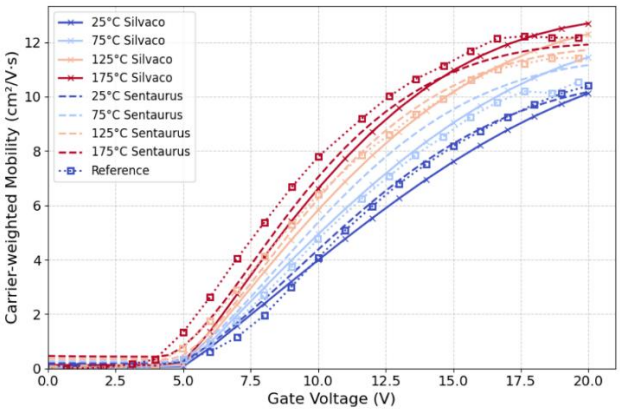


Fig. 3. Effective channel mobility, μ_{eff}, as a function of gate voltage, V_G, for a P-well doping concentration of 1.0×10^{18} cm^{-3}, showing the temperature-dependent behaviour from 25 °Cto 175 °Ctogether with the reference data reported in [4].

- **High V_G (strong inversion)** - At higher gate bias, however, the component analysis shows a clear crossover in the dominant limiting mechanism. Around $V_G \approx 14$ V, the surface-phonon-limited mobility becomes lower than the Coulomb-limited mobility, indicating that surface-phonon scattering becomes the dominant mobility-limiting contribution in the high V_G regime. The final saturation behaviour of the effective mobility is therefore set primarily by the surface-phonon term, while remote Coulomb scattering remains a secondary but still relevant limitation.

The surface-roughness component decreases with increasing gate bias, consistent with stronger carrier confinement near the SiC/SiO_2 interface, but it remains higher than both the Coulomb- and phonon-limited mobilities throughout the bias range shown. Surface roughness therefore does not emerge as the dominant limiting mechanism in this lowest-doped case. Likewise, the bulk mobility remains much larger than all interface-related components and is not limiting. This interpretation is also broadly consistent with Hall-analysis-based studies of 4H-SiC MOSFET channels, which report Coulomb-scattering dominance in weak inversion and phonon/surface-related limitations under strong inversion [16]. The reliability of this decomposition is supported by the sequential calibration procedure described in Section IV, in which bulk, SR/SP, and RCS parameters were

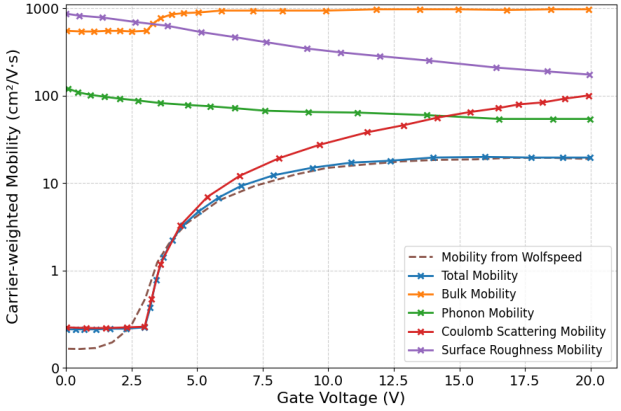


Fig. 4. Carrier-weighted effective mobility μ_{eff}as a function of gate voltage V_G for the representative lowest-doped P-well case, showing the extracted mobility components and their Matthiessen's-rule combination.

each constrained against separate, non-overlapping regions of the VG characteristic, preventing mutual compensation between components.

VI. Conclusion

This paper presented and calibrated a four-component channel-mobility framework for 4H-SiC MOSFETs in TCAD, in which the effective channel mobility is described by the harmonic combination of bulk mobility, surface-roughness scattering, surface-phonon scattering, and remote Coulomb scattering. The framework was implemented in both Synopsys Sentaurus and Silvaco using the native mobility models and remote Coulomb scattering equations available in each tool, while a common carrier-weighted extraction procedure was used to evaluate the effective inversion-layer mobility.

The calibrated parameter sets reproduced the published effective-mobility characteristics over a P-well doping range of approximately 3.6×10^{17} to 1.0×10^{18} cm^{-3} and over a temperature range from $25\,^{\circ}\mathrm{C}$ to $175\,^{\circ}\mathrm{C}$. Both TCAD implementations captured the expected doping-dependent separation of the $\mu_{\mathrm{eff}} - V_G$ curves, together with the corresponding temperature dependence of the mobility level and saturation behaviour. The component analysis further showed that, for the representative lowest-doped case, remote Coulomb scattering dominates the weak and moderate inversion regimes, while surface-phonon scattering becomes the dominant limiting mechanism at higher gate bias after sufficient screening of the Coulomb contribution. Surface roughness remains a secondary limitation in this case, and the bulk mobility is non-limiting throughout. These results support the physical consistency of the calibrated model and clarify how the measured effective mobility is reproduced across the operating range. Overall, the results demonstrate that the proposed four-component framework provides a consistent and physically meaningful basis for predictive inversion-layer mobility modelling in 4H-SiC MOSFET TCAD workflows.

The cross-tool consistency demonstrated here has direct implications for predictive TCAD-based device development. Since Sentaurus and Silvaco implement the same physical framework through different internal model structures, parameter precedence rules, and numerical discretisation schemes, obtaining consistent results requires careful alignment of both the model selection and the non-mobility physics settings. The calibrated parameter sets reported in Table I, together with the carrier-weighted extraction procedure described in Section II, provide a reproducible starting point for inversion-layer mobility modelling in 4H-SiC MOSFETs that can be transferred between the two platforms. The observed deviations near the turn-on region and at high gate bias highlight the sensitivity of the extracted mobility to interface-charge assumptions and suggest that further improvement in predictive accuracy likely requires α more precise characterisation of the fixed charge density and interface trap distribution at the SiC/SiO_2 interface.

VII. References

[1] P. Sharmila, D. Haripriya, C. Sivamani, et al., "Silicon carbide MOSFETs: A critical review of applications, technological advancements and future perspectives," Micro and Nanostructures, Art. no. 208126, 2025.

[2] T. Kimoto and J. A. Cooper, Fundamentals of Silicon Carbide Technology: Growth, Characterization, Devices and Applications. Hoboken, NJ, USA: Wiley, 2014.

[3] H. Linewih, S. Dimitrijev, and K. Y. Cheong, "Channel-carrier mobility parameters for 4H-SiC MOSFETs," Microelectronics Reliability, vol. 43, no. 3, pp. 405–411, 2003.

[4] H. Dixit, D. J. Lichtenwalner, A. Scholze, et al., "Revised channel mobility model for predictive TCAD simulations of 4H-SiC MOSFETs," Solid State Phenomena, vol. 358, pp. 103–107, 2024.

[5] A. G. Sabnis and J. T. Clemens, "Characterization of the electron mobility in the inverted ⟨100⟩ Si surface," in IEDM Tech. Dig., 1979, pp. 18–21.

[6] S. C. Sun and J. D. Plummer, "Electron mobility in inversion and accumulation layers on thermally oxidized silicon surfaces," IEEE Trans. Electron Devices, vol. 27, no. 8, pp. 1497–1508, 1980.

[7] S. Takagi, A. Toriumi, M. Iwase, and H. Tango, "On the universality of inversion layer mobility in Si MOSFETs: Part I—effects of substrate impurity concentration," IEEE Trans. Electron Devices, vol. 41, no. 12, pp. 2357–2362, 1994.

[8] C. Lombardi, S. Manzini, A. Saporito, and M. Vanzi, "A physically based mobility model for numerical simulation of nonplanar devices," IEEE Trans. Comput.-Aided Des. Integr. Circuits Syst., vol. 7, no. 11, pp. 1164–1171, 1988.

[9] V. Uhnevionak, A. Burenkov, C. Strenger, G. Ortiz, E. Bedel-Pereira, V. Mortet, F. Cristiano, A. J. Bauer, and P. Pichler, "Comprehensive study of the electron scattering mechanisms in 4H-SiC MOSFETs," IEEE Trans. Electron Devices, vol. 62, no. 8, pp. 2562–2570, 2015.

[10] Synopsys, Inc., Sentaurus Device User Guide, ver. W-2024.09, Sep. 2024.

[11] Silvaco, Inc., Victory Device User Manual. Santa Clara, CA, USA, Jun. 17, 2024.

[12] H. Dixit, D. J. Lichtenwalner, A. Scholze, et al., "Temperature dependent mobility model for predictive TCAD simulations of 4H-SiC," in Materials Science Forum, vol. 1090, pp. 153–157, 2023.

[13] D. B. M. Klaassen, "A unified mobility model for device simulation—I. Model equations and concentration dependence," Solid-State Electronics, vol. 35, no. 7, pp. 953–959, 1992.

[14] D. B. M. Klaassen, "A unified mobility model for device simulation—II. Temperature dependence of carrier mobility and lifetime," Solid-State Electronics, vol. 35, no. 7, pp. 961–967, 1992.

[15] S. Potbhare, G. Pennington, N. Goldsman, J. M. McGarrity, and A. Lelis, "Characterization of 4H-SiC MOSFET interface trap charge density using a first-principles Coulomb scattering mobility model and device simulation," in Proc. SISPAD, 2005.

[16] S. Das et al., "Study of carrier mobilities in 4H-SiC MOSFETs using Hall analysis," Materials, vol. 15, no. 19, Art. no. 6736, 2022.